

© 2024 IEEE. Personal use of this material is permitted. Permission from IEEE must be obtained for all other uses, including reprinting/republishing this material for advertising or promotional purposes, collecting new collected works for resale or redistribution to servers or lists, or reuse of any copyrighted component of this work in other works. This work has been submitted to the IEEE for possible publication. Copyright may be transferred without notice, after which this version may no longer be accessible.

Energy-Cautious Designation of Kinematic Parameters for a Sustainable Parallel-Serial Heavy-Duty Manipulator Driven by Electromechanical Linear Actuator

Alvaro Paz*, Mohammad Bahari, and Jouni Mattila
 Faculty of Engineering and Natural Sciences, Tampere University, 33720, Finland
 *Email: alvaro.pazanaya@tuni.fi

Abstract— Electrification, a key strategy in combating climate change, is transforming industries, and off-highway machines (OHM) will be next to transition from combustion engines and hydraulic actuation to sustainable fully electrified machines. Electromechanical linear actuators (EMLAs) offer superior efficiency, safety, and reduced maintenance, and they unlock vast potential for high-performance autonomous operations. However, a key challenge lies in optimizing the kinematic parameters of OHMs' on-board manipulators for EMLA integration to exploit the full capabilities of actuation systems and maximize their performance. This work addresses this challenge by delving into the structural optimization of a prevalent closed kinematic chain configuration commonly employed in OHM manipulators. Our approach aims to retain the manipulator's existing capabilities while reducing its energy expenditure, paving the way for a greener future in industrial automation, one in which sustainable and high-performing robotized OHMs can evolve. The feasibility of our methodology is validated through simulation results obtained on a commercially available parallel-serial heavy-duty manipulator mounted on a battery electric vehicle. The results demonstrate the efficacy of our approach in modifying kinematic parameters to facilitate the replacement of conventional hydraulic actuators with EMLAs, all while minimizing the overall energy consumption of the system.

Index Terms – Electromechanical linear actuator (EMLA), geometrical optimization, heavy-duty manipulator, off-highway machines (OHMs) electrification, sustainable automation.

NOMENCLATURE

List of Abbreviations

ADC Analog-to-digital converter
BEV Battery electric vehicle
EHLA Electrohydraulic linear actuator
EMLA Electromechanical linear actuator
ID Inverse dynamics
OHM Off-highway machine
PMSM Permanent magnet synchronous motor
TCP Tool center point

List of Symbols

ν Twist vector
 Ξ General decision variable
 ξ Particular decision variable
 B Matrix basis function
 c Control points

G Homogeneous transformation matrix
 J Manipulator Jacobian
 x_r Reference trajectory to track
 P Park transformation matrix
 $\ddot{\theta}_m$ Electric motor angular acceleration (rad/s²)
 $\dot{\nu}$ Spatial acceleration vector
 \dot{J} Time derivative of the manipulator Jacobian
 \dot{v}_x Linear acceleration of the EMLA (m/s²)
 η_{EMLA} EMLA mechanism efficiency
 ω_e Electric angular velocity (rad/sec)
 ω_m PMSM angular velocity (rad/sec)
 Φ_{PM} Permanent magnet linkage flux in motor (Wb)
 $\psi \psi_1 \psi_2$ Passive-joints angular offsets (rad)
 ρ Screw mechanism lead (m)
 Σ_i Spatial reference frame
 τ_m Electric motor electromagnetic torque (N · m)
 τ_m Rotor friction (N · m)
 $\theta \theta_1 \theta_2$ Passive-joints angular positions (rad)
 b_f Screw mechanism friction coefficient (N · s/m)
 $\cos(\phi)$ Electric motor power factor
 f Cost function
 f_{sm} Force applied to the screw mechanism (N)
 f_x EMLA output force (N)
 G Gear ratio ($G > 1$)
 i_d Electric motor current in d-axis (A)
 i_q Electric motor current in q-axis (A)
 I_{LL} Line-to-line current of 3-ph electric motor (A)
 J_m Rotor inertia (kg · m²)
 L First upper link length (m)
 L_1 Second upper link length (m)
 L_c First lower link length (m)
 L_d Electric motor inductance in d-axis (H)
 L_q Electric motor inductance in q-axis (H)
 L_{c0} Second lower link length (m)
 M_{sm} Screw mechanism mass (kg)
 p Number of pole pairs
 $q q_1 q_2$ Internal trigonometric angles (rad)
 R_s Electric motor stator resistance (Ω)
 t_0 Initial time (sec)
 t_m Final time (sec)
 $V_a V_b V_c$ Three-phase electric motor voltage in (V)
 $V_d V_q$ Electric motor voltage in dq-axis (V)
 V_{LL} Line-to-line voltage of 3-ph electric motor (V)
 v_x Linear velocity of the EMLA (m/s)

This work was supported by the Business Finland partnership project "Future all-electric rough terrain autonomous mobile manipulators" (Grant #2334/31/2022).

I. INTRODUCTION

A. Background and Context

The transition to zero-emission solutions is reshaping the logistics and transportation industries, particularly in urban environments, where stringent regulations are driving the move away from internal combustion engines (ICEs) [1]. A prime example of this trend is Stockholm, Sweden, which is set to implement a stringent ban on diesel engines, including trucks with cranes, by the end of 2024. This initiative is part of a broader effort to establish low-emission zones across Europe, driven by urban vehicle access regulations (UVARs) intended to improve air quality and reduce congestion [2]. Mirroring this shift towards zero-emission solutions in urban settings, the field of off-highway machines (OHMs) is also undergoing significant changes. Driven by stringent environmental regulations, such as the Paris Agreement of 2015 [3], and the push for reduced carbon footprints, the electrification of OHMs is transforming heavy-duty machinery, promising enhanced automation and sustainability, as well as greener future in this industry [4]. To address the challenges and opportunities presented by the trend of electrification, technological advancements in actuator systems are essential [5]. Currently, hydraulic linear actuators and pumps are employed in truck-mounted material handling cranes, hook and tail lifts. Hiab has already introduced an innovative solution in which the hydraulic pump is controlled by a permanent magnet synchronous motor (PMSM), marking a significant step toward electrification and sustainability in OHMs. While this represents progress, hydraulic actuators still present limitations. Although hydraulic actuators provide superior power density, they are constrained by issues such as energy inefficiency and susceptibility to leakages. Moreover, they require an additional energy conversion from electric power to hydraulic flow, which is then converted to mechanical motion. As a result, this has led to further innovation in the form of electromechanical linear actuators (EMLAs). EMLAs are an emerging technology also for heavy-duty linear actuation mechanisms, with required output forces ranging from 100 kN to 500 kN; compared to hydraulics, they offer superior efficiency and have lower maintenance requirements [6]. EMLAs could enable more effective use of the limited stored energy in battery electric vehicles (BEV), offering a direct drive system that avoids the energy conversion losses inherent in hydraulic systems and a potentially extended range despite their tasks involving heavy-weight cargo lifting and handling [7]. The compositions of both EMLAs and the electro-hydraulic linear actuator (EHLA) introduced by Hiab are illustrated in Fig. 1. As urban areas implement ambitious emission reduction plans, integrating EMLAs into machinery aligns more closely with their environmental goals, offering a more sustainable and efficient solution for high-performance and autonomous operations. However, achieving the benefits of EMLA hinges on successfully integrating EMLAs into existing OHMs' manipulator structures, ensuring not only that the new actuators seamlessly fulfill the task requirements previously handled by the conventional actuation mechanism

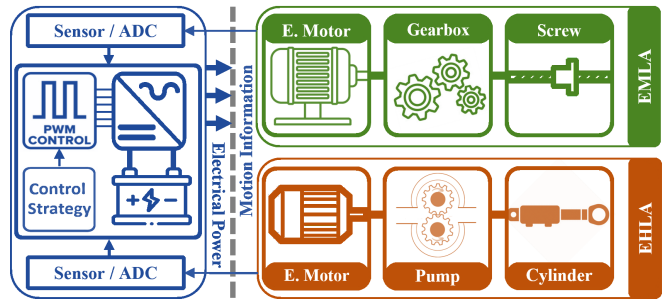


Fig. 1: The composition of an EMLA and an HLA.

of the manipulator but also that EMLAs' efficiencies are at the peak and actuation mechanism energy consumption is at lowest to conduct the tasks. Accordingly, optimizing the kinematic parameters of manipulators to find the optimal structure is crucial to implement these electric actuators. Structural optimization has emerged as a powerful tool in manipulator design [8], offering a systematic approach to identifying the most efficient configuration within a vast design space. This field has garnered significant research interest in recent years, leading to the development of robust computer-aided optimization algorithms. Significant results have been reported in the structural design of heavy-duty robots, where high-performance numerical toolboxes (e.g., ANSYS Workbench and ADAMS software) have been employed to provide a representation of rigid multibody dynamics [8], [9] while the objective functions are targeted mainly to optimize structural deformation, harmonic response or mechanical stress. Such characteristics are crucial to study when considering heavy-duty machinery. In addition, parameter optimization design has been implemented to find spring values in a loaded balance system to minimize the consumption of joint drive [10] in a 5-DoF heavy-duty manipulator.

In the context of manipulator design, optimization focuses on defining the optimal geometric parameters to ensure effective performance across the desired range of motion. Because actuators play a critical role in the manipulator's lifting capacity, structural optimization aims to minimize peak actuator force within the operational range. This translates to a reduction in the required actuator capacity, leading to a more efficient and potentially lighter manipulator design. Given the vast design space explored through structural optimization, achieving mathematically optimal solutions can be computationally expensive. While achieving mathematically optimal solutions for manipulator design is theoretically possible through optimization algorithms or analytical methods, practical considerations often necessitate alternative approaches. Shoup [11] utilized the golden section search for the min-max force problem. However, for real-world manipulator models, computationally efficient methods, such as the sequential quadratic programming (SQP) method implemented in MATLAB's f_{minmax} function, are typically employed [12]. These methods may require modifications,

such as incorporating exact merit functions alongside the Brayton [12] and Beiner [13] merit function.

B. Paper Contributions

This work addresses the critical challenge of integrating EMLAs into existing heavy-duty manipulator structures for sustainable OHM design. The key contributions of this paper are itemized as follows: leftmargin=0.35cm

- Developed a mathematical model of EMLA mechanism and subsequently computed efficiency maps as a function of force and linear velocity at the load side.
- Introduced a high-fidelity analytical model of full parallel-serial manipulator dynamics, surpassing limitations of previous studies (e.g., [8], [9], and [10])
- Rather than analyze the structural stress or harmonic response, we developed an energy-centric optimization framework prioritizing energy consumption minimization to enhance the performance and sustainability of electrified OHM.
- Developed elegant analytical solutions for solving optimal problems when considering particular examples of robots and constraints [13]. However, our solution includes the full nonlinear dynamics model of the manipulator and its nonlinear constraints; thus, by transcribing the optimal problem, a discretized version is generated than can be solved with nonlinear numerical solvers.
- Proposed an optimization method to determine optimal kinematic parameters for a prevalent closed-kinematic chain manipulator configuration, enabling efficient EMLA integration and unlocking the potential of electrification while maintaining economic viability due to the reduced energy consumption of the actuation mechanism.
- Demonstrated the potential of this research to significantly reduce the overall environmental impact of transportation and logistics by facilitating the transition from ICEs to clean electric EMLAs in heavy-duty BEVs.

Fig. 2 visualizes the organization and methodology of the paper for energy-cautious manipulator kinematic parameter optimization.

II. EMLA MATHEMATICAL MODEL

In this section, we investigate the mathematical model of an EMLA equipped with a PMSM, aiming to generate force (f_x) and linear velocity (v_x) at the load side of the actuator. The fundamental elements of an EMLA include an electric motor, gearbox, and screw mechanism, where the former provides torque and angular speed, the gearbox trades speed for increased torque, and the screw mechanism converts rotational motion into linear movement. This movement's force and velocity are functions of the gear ratio and screw's lead [14]. The main structural components of an EMLA is illustrated in Fig. 3. The power transmission sequence of the EMLA commences with (a) electric power into electromagnetic power, as described in (1)-(3), where subscripts d and q indicate the parameters in the dq frame;

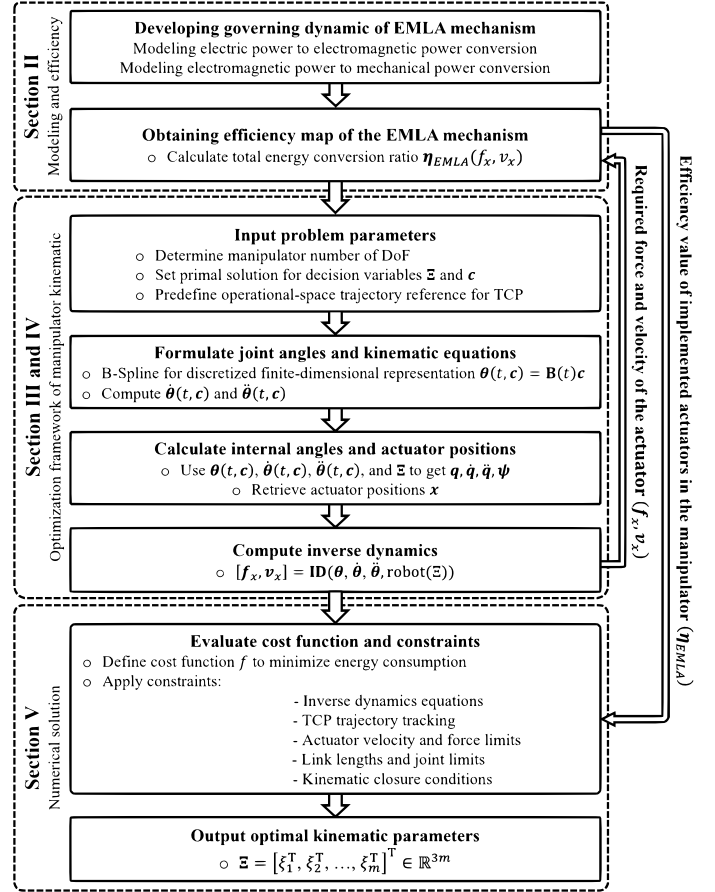


Fig. 2: Procedural flowchart illustrating the methodology for energy-cautious manipulator kinematic parameter optimization.

(b) electromagnetic power into mechanical rotation, as explained in (4), where subscripts m , sm , and f denote the parameters related to the electric motor, screw mechanism, and friction, respectively; and (c) rotational movement into linear movement, as expressed in (5), where subscript x shows the parameters at the load side. Power conversion occurs within the rotating dq reference frame, employing Park transformations (P) to decouple the three-phase system into orthogonal components, as detailed in (1) and (2). In addition, the voltages and electromagnetic torque generated by the PMSM as a function of stator currents and permanent magnet flux are obtained as (3). In the dq -axis, an equivalent model of the PMSM is illustrated in Fig. 4 [15].

$$P = \begin{bmatrix} \cos(\omega_e t) & \cos(\omega_e t - \frac{2\pi}{3}) & \cos(\omega_e t + \frac{2\pi}{3}) \\ -\sin(\omega_e t) & -\sin(\omega_e t - \frac{2\pi}{3}) & -\sin(\omega_e t + \frac{2\pi}{3}) \\ \frac{1}{2} & \frac{1}{2} & \frac{1}{2} \end{bmatrix} \quad (1)$$

$$\begin{bmatrix} V_d \\ V_q \\ V_0 \end{bmatrix} = \frac{2P}{3} \begin{bmatrix} V_a \\ V_b \\ V_c \end{bmatrix} \quad (2)$$

$$\begin{cases} V_d = R_s i_d + L_d \frac{di_d}{dt} - p\omega_m L_q i_q \\ V_q = R_s i_q + L_q \frac{di_q}{dt} + p\omega_m (L_d i_d + \Phi_{PM}) \\ \tau_m = \frac{3}{2} p i_q [\Phi_{PM} + (L_d - L_q) i_d] \end{cases} \quad (3)$$

$$\tau_m - \tau_f = J_m \ddot{\theta}_m + \tau_{sm} \quad (4)$$

$$\begin{cases} \tau_{sm} = \frac{\rho}{2\pi G} f_{sm} \\ f_x = f_{sm} - M_{sm} \dot{v}_x - b_f v_x \end{cases} \quad (5)$$

The overall efficiency of the EMLA system is determined by the ratio of mechanical power output to electrical power input. As expressed in (6), the system efficiency, η_{EMLA} , is a function of time, load force f_x , and load velocity v_x . Fig. 5 illustrates the efficiencies of the EMLAs, which will be integrated as joint drives for the heavy-duty manipulator.

$$\eta_{\text{EMLA}}(f_x, v_x, t) = \frac{f_x(t) \cdot v_x(t)}{\sqrt{3} V_{LL}(t) I_{LL}(t) \cos \phi} \quad (6)$$

III. STRUCTURE OF PARALLEL MECHANISM

Heavy-duty parallel-serial manipulators are composed of prismatic, rotational and parallel mechanisms. Geometrically, this type of parallel mechanism under study is a one-degree of freedom (DoF) closed kinematic chain of four links with lengths L, L_1, L_c , and $L_{c0} > 0$ as shown in Fig. 6. It is articulated by three passive rotational joints with angles θ, θ_1 , and θ_2 and one actuated prismatic joint with linear position x . Such passive joints are placed at the origin of frames Σ_{B1}, Σ_{B3} , and Σ_{T2} and the actuated one at Σ_{B4} . Kinematically, this parallel mechanism can be studied as two serial kinematic chains restricted by holonomic constraints. Let us now define the following reference-frame sequences for each serial kinematic chain, which we call upper and lower. For the upper serial kinematic chain, the reference frames are $\Sigma_{B0}, \Sigma_{B1}, \Sigma_{T1}$, and Σ_E , and for the lower one, $\Sigma_{B2}, \Sigma_{B3}, \Sigma_{B4}, \Sigma_P$, and Σ_{T2} . At the beginning and end of the closed kinematic chain, general reference frames can be placed, such as

$$\Sigma_{Bc} = \Sigma_{B0} = \Sigma_{B2} \quad \text{and} \quad \Sigma_{Tc} = \Sigma_{T1} = \Sigma_{T2} \quad (7)$$

As shown in Fig. 6, the origins of the reference frames Σ_{B1}, Σ_{Bc} , and Σ_{Tc} are the vertices of a triangle parameterized by link lengths and joint configurations. The inner

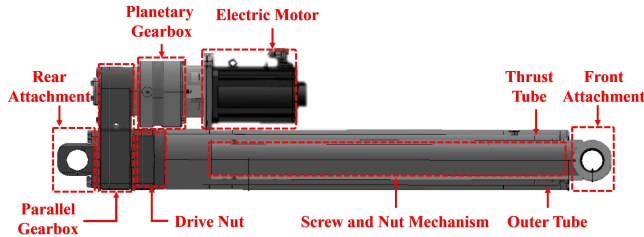


Fig. 3: The structure of an EMLA.

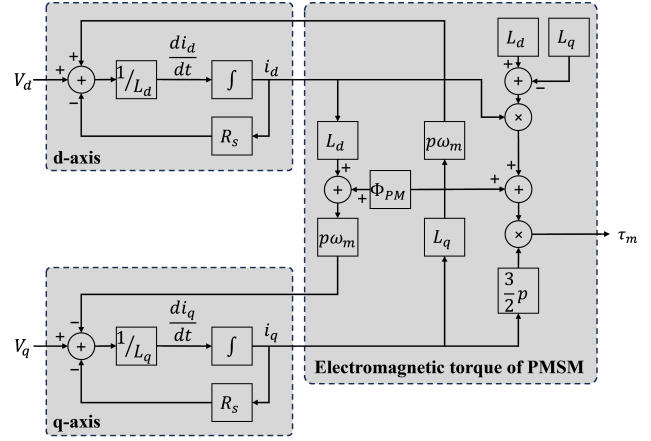


Fig. 4: Equivalent model of a PMSM in the d-q reference frame

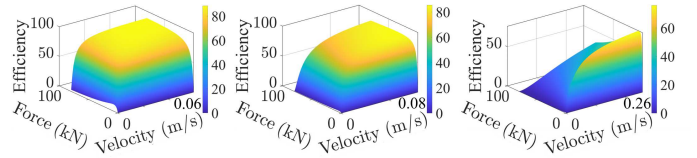


Fig. 5: Efficiency of EMLAs as the function of force and linear velocity at load side

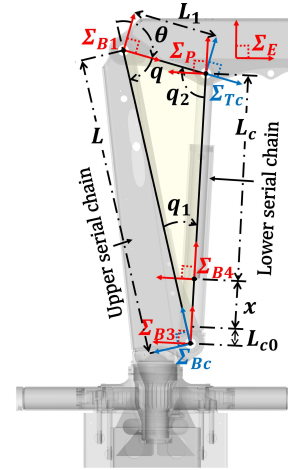


Fig. 6: The parallel mechanism composed of three passive rotational joints and one linearly actuated joint. It can be kinematically analyzed as two separated serial chains, upper and lower, which meet in the reference frames Σ_{Bc} and Σ_{Tc} . Each of the rotational joints has an associated internal angle, an offset angle, and a joint configuration angle. Such angles and their time derivatives are essential to solving the mechanism trigonometry, kinematics, and dynamics.

angles of this triangle are denoted by q, q_1 , and q_2 , which are angles around the screw axis of the motion of the reference frames Σ_{B1}, Σ_{Bc} , and Σ_{Tc} , respectively. Such inner angles hold the triangle property

$$q + q_1 + q_2 = -\pi \quad (8)$$

and they can be computed once the link lengths and piston

position $x \geq 0$ are given using the expressions [16]

$$q = -\arccos\left(\frac{(x+x_0)^2 - L^2 - L_1^2}{-2LL_1}\right) \quad (9a)$$

$$q_1 = -\arccos\left(\frac{L_1^2 - (x+x_0)^2 - L^2}{-2(x+x_0)L}\right) \quad (9b)$$

$$q_2 = -\arccos\left(\frac{L^2 - (x+x_0)^2 - L_1^2}{-2(x+x_0)L_1}\right) \quad (9c)$$

where $x_0 = L_c + L_{c0}$.

Therefore, the passive joint angles can be calculated by

$$\theta = q + \psi, \quad \theta_1 = q_1 + \psi_1, \quad \theta_2 = q_2 + \psi_2 \quad (10)$$

where ψ , ψ_1 , and ψ_2 are offset angles that are constant scalar functions with respect to x but not with respect to link length.

The geometric closure of the parallel mechanism is forced through holonomic constraints by the following expressions for internal angular velocities \dot{q} , \dot{q}_1 , and \dot{q}_2 as linear functions of the linear velocity of the actuator \dot{x} .

$$\dot{q} = k_1 \dot{x} \quad \dot{q}_1 = k_2 \dot{x} \quad \dot{q}_2 = k_3 \dot{x} \quad (11)$$

where

$$k_1 = -(x + x_0) / (LL_1 \sin q) \quad (12a)$$

$$k_2 = -(x + x_0 - L \cos q_1) / (x + x_0)L \sin q_1 \quad (12b)$$

$$k_3 = -(x + x_0 - L_1 \cos q_2) / (x + x_0)L_1 \sin q_2 \quad (12c)$$

with q , q_1 , and $q_2 \neq 0$. As well, internal angular accelerations \ddot{q} , \ddot{q}_1 , and \ddot{q}_2 are found by deriving (11) with respect to time as

$$\ddot{q} = \dot{k}_1 \dot{x} + k_1 \ddot{x} \quad \ddot{q}_1 = \dot{k}_2 \dot{x} + k_2 \ddot{x} \quad \ddot{q}_2 = \dot{k}_3 \dot{x} + k_3 \ddot{x} \quad (13)$$

where \dot{k}_1 , \dot{k}_2 , and \dot{k}_3 are the time derivatives of (12) and \ddot{x} is the actuator's linear acceleration.

In addition, the angular velocities of passive joints $\dot{\theta}$, $\dot{\theta}_1$, and $\dot{\theta}_2$ are obtained by deriving (10) with respect to time as

$$\dot{\theta} = \dot{q}, \quad \dot{\theta}_1 = \dot{q}_1, \quad \dot{\theta}_2 = \dot{q}_2 \quad (14)$$

and their angular accelerations as

$$\ddot{\theta} = \ddot{q}, \quad \ddot{\theta}_1 = \ddot{q}_1, \quad \ddot{\theta}_2 = \ddot{q}_2 \quad (15)$$

By adopting a screw theory notation [17], from definition (7), it is assumed that reference frames Σ_{B0} and Σ_{B2} have the same transformation matrices $\mathbf{G}_{Bc} = \mathbf{G}_{B0} = \mathbf{G}_{B2} \in SE(3)$, twist vectors $\mathbf{v}_{Bc} = \mathbf{v}_{B0} = \mathbf{v}_{B2} \in se(3)$, and spatial accelerations $\dot{\mathbf{v}}_{Bc} = \dot{\mathbf{v}}_{B0} = \dot{\mathbf{v}}_{B2} \in se(3)$. Likewise, reference frames Σ_{T1} and Σ_{T2} have the same kinematic features as reference frame Σ_{Tc} . For more kinematic details using Lie groups and their algebras, see [18].

IV. KINEMATIC PARAMETERS OPTIMIZATION PROBLEM

The optimization problem can be formulated as follows. Given an n -DoF heavy-duty parallel-serial manipulator and a predefined operational-space trajectory reference for its TCP, find the optimal values for the link lengths L , L_{c0} , and L_c , for each of the parallel mechanisms, that minimizes the EMLA's energy expenditure while respecting robot constraints such as joint limits, force-and-velocity boundaries in the linear actuators, TCP reference trajectory tracking, boundaries for

link lengths, and trigonometric closure conditions for closed chains consistency. In other words, the robot must be forced to perform the same TCP trajectory reference while the numerical optimizer finds the best link lengths that minimizes the energy consumption of the EMLAs while respecting structural restrictions.

Let us now define the decision variable vector for a single parallel mechanism (see Fig. 6) as a stack of lengths

$$\boldsymbol{\xi} = [L \quad L_{c0} \quad L_c]^\top \in \mathbb{R}^3 \quad (16)$$

Thus, according to (9) and (10), the internal angles $q_1(\boldsymbol{\xi})$ and $q_2(\boldsymbol{\xi})$, the offset angles $\psi_1(\boldsymbol{\xi})$ and $\psi_2(\boldsymbol{\xi})$, and the passive joint angles $\theta_1(\boldsymbol{\xi})$ and $\theta_2(\boldsymbol{\xi})$ become functions of $\boldsymbol{\xi}$.

Let us now adopt a BSpline parameterization of the configurational space trajectory [19] to obtain a discretized finite-dimensional representation of our problem. For this a finite set of collocation points \mathcal{T} transcribes the time as

$$\mathcal{T} \triangleq \{t_0 \cdots t_k \cdots t_M\} \quad (17)$$

where, k is the iterator, and M is the number of partitions.

The vector $\boldsymbol{\theta}(t, \mathbf{c}) \in \mathbb{R}^n$ that contains only the θ values of each parallel mechanism (i.e., first element of (10)) and the joint positions of single-joint mechanisms can be defined by the matrix BSpline form

$$\boldsymbol{\theta}(t, \mathbf{c}) = \mathbf{B}(t)\mathbf{c} \quad (18)$$

where $\mathbf{B}(t) \in \mathbb{R}^{n \times nN}$ is the matrix form of basis functions and N is the number of control points stacked in $\mathbf{c} \in \mathbb{R}^{nN}$.

By time deriving the last equation twice, the following expressions for velocity and acceleration are obtained [20]

$$\dot{\boldsymbol{\theta}}(t, \mathbf{c}) = \dot{\mathbf{B}}(t)\mathbf{c} \quad (19)$$

$$\ddot{\boldsymbol{\theta}}(t, \mathbf{c}) = \ddot{\mathbf{B}}(t)\mathbf{c} \quad (20)$$

Using $\boldsymbol{\theta}$ from (18) into (10) and (9a), the actuator position x is retrieved, and then x and $\boldsymbol{\xi}$ are used to compute all remaining internal angles and passive joint angles. Additionally, all angles and x in the parallel mechanism become functions of the control points \mathbf{c} and link lengths $\boldsymbol{\xi}$.

The inverse dynamics of parallel-serial manipulators can be expressed by the function [21]

$$[\mathbf{f}_x, \mathbf{v}_x] = \mathbf{ID}(\boldsymbol{\theta}, \dot{\boldsymbol{\theta}}, \ddot{\boldsymbol{\theta}}, \text{robot}(\boldsymbol{\Xi})) \quad (21)$$

where \mathbf{f}_x and \mathbf{v}_x are the actuator forces and velocities; $\boldsymbol{\theta}$, $\dot{\boldsymbol{\theta}}$, and $\ddot{\boldsymbol{\theta}}$ are functions of \mathbf{c} ; $\text{robot}(\cdot)$ is the structure that contains all topological, kinematic, and inertial information of the robot and is a function of

$$\boldsymbol{\Xi} \triangleq [\boldsymbol{\xi}_1^\top \quad \boldsymbol{\xi}_2^\top \quad \cdots \quad \boldsymbol{\xi}_m^\top]^\top \in \mathbb{R}^{3m} \quad (22)$$

which contains link lengths of all parallel mechanisms in the manipulator; and m is the number of these mechanisms.

From previous considerations, the optimal problem to be solved takes the form of a constrained nonlinear programming problem, as follows:

$$\underset{\boldsymbol{\Xi}, \mathbf{c}}{\text{minimize}} \quad f = \frac{1}{2} \Delta_t \sum_{t=t_0}^{t_M} \left(\sum_{i=1}^{n_a} \frac{f_{x_i} \cdot v_{x_i}}{\eta_{\text{EMLA}_i}(f_{x_i}, v_{x_i})} \right)^2 \quad (23)$$

subject to

$$[\mathbf{f}_x, \mathbf{v}_x] = \mathbf{ID}(\boldsymbol{\theta}, \dot{\boldsymbol{\theta}}, \ddot{\boldsymbol{\theta}}, \text{robot}(\Xi)) \quad (24a)$$

$$\mathbf{x}_r(t) = \mathbf{G}_{tcp}(\boldsymbol{\theta}) \quad (24b)$$

$$\dot{\mathbf{x}}_r(t) = \mathbf{J}(\boldsymbol{\theta})\dot{\boldsymbol{\theta}} \quad (24c)$$

$$\ddot{\mathbf{x}}_r(t) = \dot{\mathbf{J}}(\boldsymbol{\theta}, \dot{\boldsymbol{\theta}})\dot{\boldsymbol{\theta}} + \mathbf{J}(\boldsymbol{\theta})\ddot{\boldsymbol{\theta}} \quad (24d)$$

$$\mathbf{v}_{x_{low}} \leq \mathbf{v}_x \leq \mathbf{v}_{x_{up}} \quad (24e)$$

$$\mathbf{f}_{x_{low}} \leq \mathbf{f}_x \leq \mathbf{f}_{x_{up}} \quad (24f)$$

$$0 \leq \boldsymbol{\xi} \leq \boldsymbol{\xi}_{up} \quad (24g)$$

$$\boldsymbol{\theta}_{low} \leq \boldsymbol{\theta} \leq \boldsymbol{\theta}_{up} \quad (24h)$$

$$\dot{\boldsymbol{\theta}}_{low} \leq \dot{\boldsymbol{\theta}} \leq \dot{\boldsymbol{\theta}}_{up} \quad (24i)$$

$$0 \leq x(t) \leq L_c \quad (24j)$$

$$L_{c0} + x(t) + L_c \leq L + L_1 \quad (24k)$$

$$q + q_1 + q_2 = -\pi \quad (24l)$$

$$\mathbf{G}_{T1}(\boldsymbol{\theta}) = \mathbf{G}_{T2}(\boldsymbol{\theta}) \quad (24m)$$

where $\Delta_t \triangleq t_k - t_{k-1}$; the cost function f represents the discrete time integral of the sum of the output power of EMLAS with n_a as the number of linear actuators; η_{EMLA} is the function defined in (6) which stands for EMLA efficiency; and f_{x_i} and v_{x_i} denote the scalar force and velocity of the i -th actuator, respectively. It should be noted that the cost function f stands for the energy expenditure because it is the time integral of power. The variables $\mathbf{x}_r(t)$, $\dot{\mathbf{x}}_r(t)$, and $\ddot{\mathbf{x}}_r(t)$ represent the position, velocity, and acceleration of the TCP trajectory reference in the operational space, and $\mathbf{J}(\boldsymbol{\theta})$ and $\dot{\mathbf{J}}(\boldsymbol{\theta}, \dot{\boldsymbol{\theta}})$ are the manipulator Jacobian and its time derivative, respectively. The actuator's velocity and force are bounded through (24e-24f). The upper and lower values are denoted by the subscripts *up* and *low*, respectively. Positive lengths are forced with (24g) and joint limits with (24h-24i).

The trigonometric consistency for each closed kinematic chain in the robot is achieved via the constraints (24j-24m). For instance, (24k) forces the upper chain to be longer than the lower one to avoid singularities in (9), while (24l) ensures the triangle property (8). The last constraint (24m) imposes the kinematic loop closure by forcing the upper and lower serial chains to end in the same $SE(3)$ element; see (7).

V. NUMERICAL SIMULATIONS AND RESULTS

Let us illustrate the kinematic parameter optimization problem described in the last section with a heavy-duty 7-DoF parallel-serial manipulator HIAB robot, as depicted in Fig. 7. For this study, we analyze only the motion provided by the three linear actuators, which are both closed chains and telescope joint. This simulation was implemented in Matlab with *fmincon* as the solver in a laptop endowed with standard computational capabilities, 1.80GHz, and 16Gb RAM. We set the BSpline parameters as $N = 22$, $M = 25$, and $\mathcal{T} = \{0, 0.25, \dots, 6.25\}$. Conversely, link lengths were initially set as $\boldsymbol{\xi}_1 = [1.75, 0.544, 1.27]$ for the first closed chain and $\boldsymbol{\xi}_2 = [1.75, 0.55, 1.2]$ for the second. A spiral reference trajectory in the X-Z plane was forced to track (see Fig. 7) because this shape covers most of the operational space when only the closed-loop motion is enabled. Fig. 8 and Fig. 9 illustrate the variation in decision

variables during the optimization process in the first and second closed chain accordingly, while Fig. 10 depicts the objective function value during the optimization iterations. To visualize the changes in the structure of the heavy-duty manipulator, Fig. 11 shows the topology of the manipulator with initial and optimal kinematic parameters.

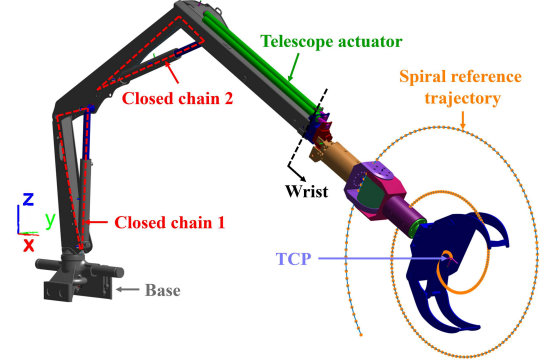


Fig. 7: Heavy-duty parallel-serial manipulator HIAB. It is a 7-DoF robot endowed with two parallel mechanisms. Its TCP is following a spiral reference trajectory that can cover a considerable area of the operational space, as its rotational base and spheric wrist are considered fixed.

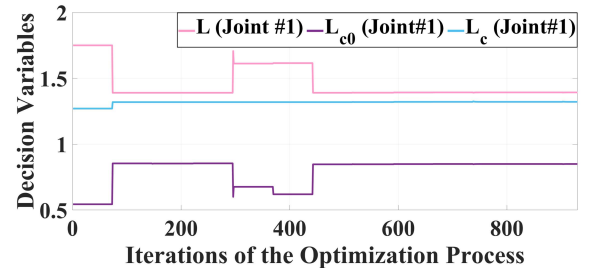


Fig. 8: Optimization results: Variation in decision variables of first closed chain in the optimization process.

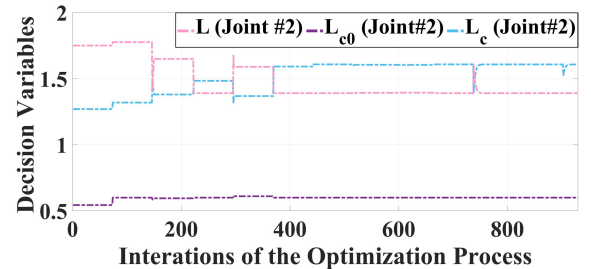


Fig. 9: Optimization results: Variation in decision variables of second closed chain in the optimization process.

VI. CONCLUSIONS

This paper presents a comprehensive approach to integrating EMLAs into heavy-duty manipulator structures for sustainable OHM design. Focusing on the structural optimization of a prevalent closed kinematic chain configuration used in heavy-duty manipulators, we have developed an energy-centric optimization framework to minimize energy consumption. This study surpasses the limitations of previous

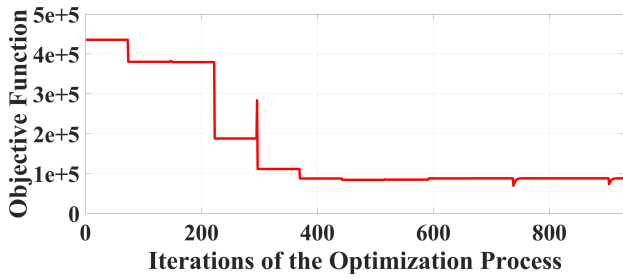


Fig. 10: Variation in the objective function during the optimization process. The amount of energy expenditure is minimized according to the expression (23) in around 900 iterations of SQP.

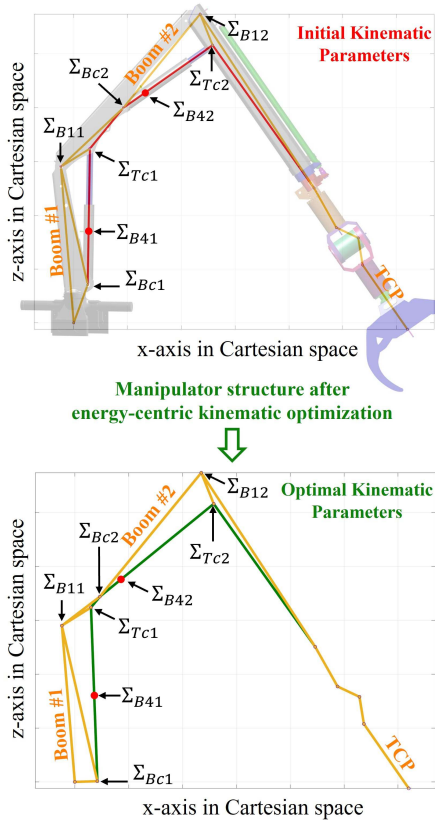


Fig. 11: Comparison among manipulator structures, which illustrates the primal solution (upper) and optimal solution (lower) when closed-loop kinematic parameters are optimized according to the optimal problem (23-24).

studies that focused solely on structural or dynamic analysis by considering the efficiency of actuation into account. By introducing a high-fidelity analytical model of the full parallel-serial manipulator dynamics, we determined optimal kinematic parameters for harmonious EMLA integration. The proposed methodology holds significant potential to reduce the environmental impact of the transportation and logistics industry by facilitating the transition from ICEs to clean-tech electric actuators in heavy-duty BEVs. Future research can explore advanced control strategies, more sophisticated EMLA models, the harmonic response and natural frequency and an analytical representation of the whole working space.

REFERENCES

- [1] Zhijie Yang, Haibo Huang, and Feng Lin. Sustainable electric vehicle batteries for a sustainable world: perspectives on battery cathodes, environment, supply chain, manufacturing, life cycle, and policy. *Advanced Energy Materials*, 12(26):2200383, 2022.
- [2] Osvaldo Navarro Lopez. Urban vehicle access regulations. *Sustainable freight transport: theory, models, and case studies*, pages 139–163, 2018.
- [3] Paris Agreement. Paris agreement. In *report of the conference of the parties to the United Nations framework convention on climate change (21st session, 2015: Paris)*. Retrived December, volume 4, page 2017. HeinOnline, 2015.
- [4] Daniele Beltrami, Paolo Iora, Laura Tribioli, and Stefano Uberti. Electrification of compact off-highway vehicles—overview of the current state of the art and trends. *Energies*, 14(17):5565, 2021.
- [5] Duc Minh Nguyen, Mustafa A. Kishk, and Mohamed-Slim Alouini. Toward sustainable transportation: Accelerating vehicle electrification with dynamic charging deployment. *IEEE Transactions on Vehicular Technology*, 71(9):9283–9296, 2022.
- [6] Andrew Turner, Keith Ramsay, Richard Clark, and David Howe. Direct-drive electromechanical linear actuator for shift-by-wire control of an automated transmission. In *2006 IEEE Vehicle Power and Propulsion Conference*, pages 1–6, 2006.
- [7] Mohammad Bahari, Alvaro Paz, Andrew S. Habib, and Jouni Mattila. Performance evaluation of an electromechanical linear actuator with optimal trajectories. In *2023 IEEE 97th Vehicular Technology Conference (VTC2023-Spring)*, pages 1–7, 2023.
- [8] Haiyan Shao, Xinle Li, Ke Qin, Weiping Liu, Guoping Li, and Tao Wu. Structural design and simulation analysis of 4-dof heavy-duty robot. In *2019 IEEE International Conference on Real-time Computing and Robotics (RCAR)*, pages 673–678, 2019.
- [9] Jing Zhang, Youqing Shen, Guangping Wu, and Hongwei Guo. Optimization design for link structure of heavy-duty transfer robot based on response surface method. In *2021 6th International Conference on Control, Robotics and Cybernetics (CRC)*, pages 6–12, 2021.
- [10] Lei Liu, Bo Huang, Yan He Zhu, and Jie Zhao. Optimization design of gravity compensation system for a 5-dof articulated heavy-duty robot. In *Mechatronics Engineering, Computing and Information Technology*, volume 556 of *Applied Mechanics and Materials*, pages 2359–2364. Trans Tech Publications Ltd, 7 2014.
- [11] Terry E Shoup and Robert A Lucas. A practical guide to computer methods for engineers. 1980.
- [12] Robert Brayton, Stephen Director, Gary Hachtel, and Luis Vidigal. A new algorithm for statistical circuit design based on quasi-newton methods and function splitting. *IEEE Transactions on Circuits and Systems*, 26(9):784–794, 1979.
- [13] L Beiner. A min-max problem of optimal actuator placement for lifting. *Robotica*, 13(6):619–622, 1995.
- [14] Wenping Cao, Barrie C Mecrow, Glynn J Atkinson, John W Bennett, and David J Atkinson. Overview of electric motor technologies used for more electric aircraft (mea). *IEEE Transactions on Industrial Electronics*, 59(9):3523–3531, 2011.
- [15] Kukhyun Ahn, Alparslan Emrah Bayrak, and Panos Y. Papalambros. Electric vehicle design optimization: Integration of a high-fidelity interior-permanent-magnet motor model. *IEEE Transactions on Vehicular Technology*, 64(9):3870–3877, 2015.
- [16] Wen-Hong Zhu. *Virtual decomposition control: toward hyper degrees of freedom robots*, volume 60. Springer Science & Business Media, 2010.
- [17] Kevin M Lynch and Frank C Park. *Modern robotics*. Cambridge University Press, 2017.
- [18] Alvaro Paz and Gustavo Arechavaleta. Analytical differentiation of the articulated-body algorithm: a geometric multilinear approach. *Multibody System Dynamics*, 60(3):347–373, 2024.
- [19] S.-H. Lee, J. Kim, F.-C. Park, M. Kim, and J.-E. Bobrow. Newton-type algorithms for dynamics-based robot movement optimization. *IEEE Transactions on Robotics*, 21(4):657–667, 2005.
- [20] Alvaro Paz and Gustavo Arechavaleta. Practical guide to solve the minimum-effort problem with geometric algorithms and b-splines. In *2019 International Conference on Robotics and Automation (ICRA)*, pages 6720–6726. IEEE, 2019.
- [21] Goran R Petrović and Jouni Mattila. Mathematical modelling and virtual decomposition control of heavy-duty parallel-serial hydraulic manipulators. *Mechanism and Machine Theory*, 170:104680, 2022.